Solar Energy 174 (2018) 640–647

Contents lists available at ScienceDirect

Solar Energy

journal homepage: www.elsevier.com/locate/solener

Absorber materials based on polymer nanocomposites containing silver nanoparticles for solar thermal collectors

Silvana V. Asmussen, Claudia I. Vallo*

Instituto de Investigaciones en Ciencia y Tecnología de Materiales (INTEMA), Universidad Nacional de Mar del Plata, CONICET, J. B. Justo 4302, 7600 Mar del Plata, Argentina

ARTICLE INFO

Keywords:
Solar thermal collectors
Absorber materials
Polymer nanocomposites
Silver nanoparticles

ABSTRACT

This study describes the synthesis and characterization of polymer-based nanocomposites to fabricate absorber materials for solar thermal collectors. Heat generation by nanosized silver particles (NSP) under irradiation with light of appropriate wavelength is exploited for an efficient harvesting of solar energy. NSP were synthesized by reduction of silver nitrate ($AgNO_3$) in a methacrylate resin. The photothermal conversion of solar energy into heat is optimized by increasing the overlap between the plasmonic band of the NSP and the spectral emission of the sun. Thus, the synthesis conditions were adjusted in order to broaden the plasmon absorption band of the resultant NSP. The UV–vis spectra of suspensions containing 300 ppm NSP exhibited a broad absorption band in the range between 360 and 1100 nm with three absorption peaks at 335, 440, and 700 nm. These absorption bands are associated to the presence of triangular NSP, which was confirmed by TEM microscopy. The resins containing NSP were activated with benzoyl peroxide and polymerized after 20 min at 80 °C. The photothermal conversion effect of the nanocomposites was assessed by monitoring the temperature increase with fine thermocouples embedded in 2-mm thick specimens during irradiation with light of different wavelength. The temperature reached during irradiation of nanocomposites showing a very broad absorption band was 115 °C while that of the nanocomposites exhibiting a single peak was 102 °C.

1. Introduction

The rising cost of fossil fuels and a growing level of environmental awareness over the past two decades have encouraged the use of solar energy in thermal applications. Solar thermal collectors are devices that convert electromagnetic solar radiation energy into heat (Tian and Zhao, 2013; Thirugnanasambandam et al., 2010; O'Hegarty et al., 2016). In general, solar collectors are classified into three categories according to the operating temperature, high temperature (≥1000 °C), intermediate temperature (~300 °C) and low temperature (≤100 °C). The most common type of low-temperature solar collectors consists of a blackened plate to absorb solar radiation and tubes containing a heat-transport fluid to remove heat from the absorber (Tian and Zhao, 2013; Thirugnanasambandam et al., 2010; O'Hegarty et al., 2016). The absorber plate is covered by a highly transmissive glass cover to allow the maximum amount of solar energy to be incident on its surface while minimizing heat losses. In addition, the plate is surrounded by insulation in order to reduce heat losses (Beikircher et al., 2015). Conventional absorber plates are fabricated from metals coated with paints, which absorb solar energy more efficiently than common black paint (Mason,1983). Alternatively, direct absorption solar collectors are a new type of solar collectors that use a suspension of nanoparticles (NNP) in a conventional base fluid (nanofluid). In these thermal collectors the solar radiation is absorbed by the suspension of NNP, which acts as both absorber and heat transfer medium (Sarsam et al., 2015). Studies on the photothermal conversion of nanofluids prepared from silver (Yu and Xuan, 2018), gold (Jeon et al., 2016; Wang et al., 2017a,b) and graphene (Fan et al., 2017) have been recently reported. Although the use of nanofluids in solar collectors has showed a good performance, there are still some issues such as the high cost of producing nanofluids as well as instability and agglomeration of the NNP that need to be addressed (Qin et al., 2017; Holm et al., 2017; Sharaf et al., 2018).

Currently, the fundamental principles that govern the performance of flat-plate collectors are well understood and significant research effort has been focussed on the development of novel materials for high-performance solar thermal collectors (Granqvist and Niklasson, 2018; Khan et al., 2018). The most important component of solar collectors is the absorber surface as it determines the speed and efficiency of photothermal conversion of solar energy into heat. Polymeric materials

* Corresponding author.
E-mail address: civallo@fi.mdp.edu.ar (C.I. Vallo).

https://doi.org/10.1016/j.solener.2018.09.062
Received 23 July 2018; Received in revised form 20 September 2018; Accepted 22 September 2018

present the advantage of both weight and cost reduction, which make them very attractive candidates for solar thermal collectors. Recent studies have described absorber materials prepared from biopolymers (Klein et al., 2017), and films of a polymer with embedded gold (Shang et al., 2017) and silver (Mishra et al., 2010; Barrera et al., 2018) NNP.

It is well known that noble metal NNP liberate heat when exposed to light. Photoexcitation of the conduction electrons of the NNP induces surface plasmon oscillations, which liberate heat as a result of non-radiative relaxation pathways (Baffou and Quidant, 2013). Although heat liberation in noble metal NNP was considered a secondary effect, over the last decade, it has been demonstrated that noble metal NNP can serve as efficient nanosources of heat giving rise to a new set of applications of technological interest such as photothermal therapy to treat cancer (Aberasturi et al., 2015) and steam generation (Wang et al., 2017a,b).

The objective of this study was the synthesis of polymeric absorber materials to be used in low-temperature solar collectors ($\leq 100\,^{\circ}C$) which consist of a plate to absorb solar radiation and tubes containing a heat-transport fluid to remove heat from the absorber. Suspensions of NSP were prepared in methacrylate monomers using acrylonitrile as stabilizer. Experimental conditions were adjusted in order to achieve a broad plasmonic band of the resultant NSP. The resins containing NSP were polymerized and the photothermal conversion effect of the resulting nanocomposites was examined.

2. Experimental

2.1. Materials

Silver nitrate ($AgNO_3$, ≥99%, Sigma Aldrich, USA). Benzoyl peroxide (BPO, ≥97%, Sigma Aldrich, USA), 2,6-di-tert-butyl-p-cresol (BHT, ≥99%, Sigma Aldrich, USA) and acrylonitrile (ACN, 99%, Sigma Aldrich, USA) were employed as received. The methacrylate resins 2,2-bis[4-(2-hydroxy-3-methacryloxyprop-1-oxy)phenyl]-propane (BisGMA, 90%) and 2,2-bis[4-(2-methacryloxyethoxy)phenyl]propane (MetB, 98%) were from Esstech, USA. Triethylene glycol dimethacrylate (TEGDMA, 95%) was from Aldrich, USA. MetA represents a mixture (70/30) BisGMA/TEGDMA weight ratio. The manufacturers add different inhibitors to the methacylate resins to prevent polymerization during storage (Asmussen and Vallo, 2015). In addition, we added 200 ppm 2,6-di-tert-butyl-p-cresol (BHT) inhibitor to the resins. As reported by the manufacturers the viscosity of MetA is 5.7 Pa·s while that of ACN is $3.4 \cdot 10^{-4}$ Pa·s. The structure of the reactants is shown in Fig. 1. Irradiation of the nanocomposites was carried out with light emitting diodes (LEDs) with its irradiance centred at 410, 465, 520 and 630 nm (D + LED, Argentina). Specimens used in photothermal conversion studies were irradiated by the LED placed at 5 mm from the specimen surface. The power emitted by the LEDs at a distance of 5 mm was set equal to 50 mW. In addition, a white 7 W LED (Osram, BO-F7OSKD) was used.

2.2. Preparation of NSP

$AgNO_3$ was first dissolved in ACN at silver mass fraction equal to 3 wt% (solution M). Suspensions of NSP were prepared from blends of 1 g of solution M and the appropriate amount of MetA. NSP were synthesized in MetA by reduction of $AgNO_3$ by the polymerization inhibitors present in the resin (Asmussen and Vallo, 2015). Specimens for photothermal conversion studies were also prepared from suspensions of spherical NSP in MetB resin. Details of the synthesis of spherical NSP were reported elsewhere (Asmussen and Vallo, 2015). Photothermal conversion in nanocomposites derived from these suspensions were used in this study for comparative purposes.

2.3. Characterization studies

UV–vis absorption spectra were acquired with a 1601 PC Shimadzu spectrophotometer. Sample preparation was described elsewhere (Asmussen and Vallo, 2015). The formation of NSP at temperatures higher than room temperature was monitored using a temperature-controlled sample holder accessory of the UV–visible spectrophotometer.

The morphology of the NSP was examined by electron microscopy (Philips CM-12 transmission electron microscope). Samples were prepared as described elsewhere (Asmussen and Vallo, 2015).

2.4. Polymerization of resins containing NSP

Polymerization of suspensions of NSP in MetA was monitored by Fourier transform infrared in the near range (NIR) using a Nicolet 6700 Thermo Scientific spectrophotometer. Polymerization of resins containing NSP and activated with 1 wt% BPO, was carried out at 80 ± 2 °C. The degree of conversion was assessed by monitoring the band assigned to the methacrylate functional group (6165 cm^{-1} in the NIR).

2.5. Temperature measurements

Photothermal conversion effects were examined by monitoring temperature changes during irradiation of nanocomposite materials with the light sources described in item 2.1. The temperature was monitored with fine thermocouples (K-type, Omega Engineering Inc., USA, precision ± 0.5 °C) inserted in 2 mm thick specimens. The diameter of the specimens was either 10 or 20 mm. The thermocouple was placed carefully in the middle of the thickness and then the assembly was placed in the oven at 80 °C to polymerize the resins.

3. Results and discussion

3.1. Preparation and characterization of NSP

NSP were synthesized by reduction of $AgNO_3$ in MetA methacrylate resin. The reducing agents of the silver ions were the inhibitors added to the resin to avoid premature polymerization (Asmussen and Vallo, 2015). $AgNO_3$ is not soluble in the methacrylate resin; therefore it was first dissolved in a small amount of ACN and this solution was added the MetA in the proportions shown in Table 1. ACN polymerizes during the cure of the resins and, therefore, it is not necessary to remove it by evaporation.

Suspensions of NSP were prepared by mixing 1 g of a 3 wt% solution of $AgNO_3$ in ACN with the required amount of MetA. The viscosity of MetA is 5.7 Pa·s while that of ACN is $3.4 \cdot 10^{-4}$ Pa·s. Increasing the amount of NSP the proportion of BHT reducer agent present in the MetA decreases while the mobility of the reacting medium increases as a result of the increased proportion of the low-viscosity ACN.

It is well known that silver ions can react with some alkene molecules, in a reversible way, to form silver-alkene complexes (Hong et al., 2000; Zhang and Han, 2003). The interaction between Ag^+ ions with ACN is described as follows:

$$Ag^+ + 2\ H_2C{=}CHCN \rightleftharpoons \left[Ag\left(H_2C{=}CHCN\right)_2\right]^+$$

The reduction of silver ion by BHT is illustrated in the following reaction scheme:

$$\left[Ag\left(H_2C{=}CHCN\right)_2\right]^+ + H^{\bullet} \longrightarrow \left[\underset{\text{atomic}}{Ag}\left(H_2C{=}CHCN\right)_2\right] + H^+$$

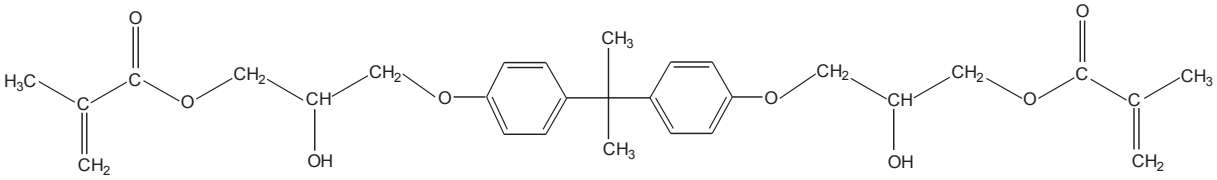

BisGMA

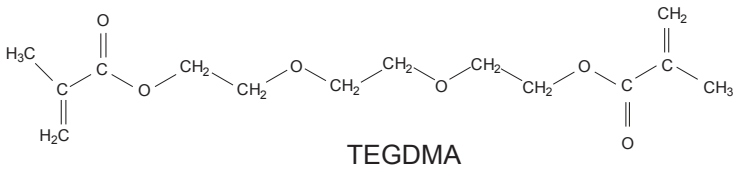

TEGDMA

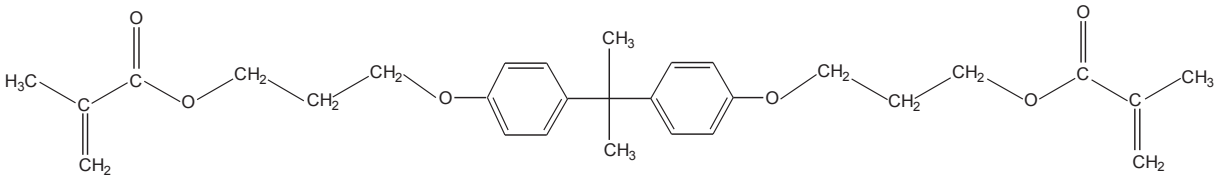

MetB

Fig. 1. Chemical structure of the resins.

Table 1
Proportion of reactants used in the preparation of dispersions of silver NSP in MetA.

ppm Ag	wt% Ag	g total/g ACN	g MetA/g ACN
150	0.015	200	199
250	0.025	120	119
300	0.03	100	99
1000	0.1	30	29
2000	0.2	15	14

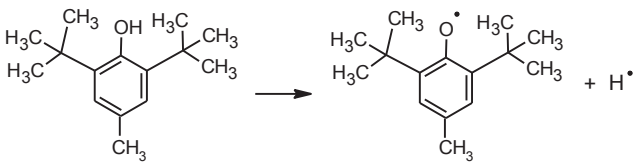

The kinetics of formation of NSP was examined by UV–vis spectroscopy. Noble metals nanoparticles (typically gold, silver or platinum) exhibit charge density oscillations known as localized surface plasmons. UV–vis absorption spectra obtained at different times in mixtures containing 150 ppm $AgNO_3$ are presented in Fig. 2. The plasmonic band associated to the NSP appeared after mixing the reagents at room temperature. The process was completed in about 24 h and yielded a single absorption band centred at 440 nm indicating the formation of spherical NSP. ACN plays an important role as stabilizer; clear suspensions were obtained only in its presence, whereas precipitated silver resulted in its absence (Asmussen and Vallo, 2015). UV–vis spectra of suspensions containing up to ~250 ppm NSP gave a single absorption band at ~440 nm. On the other hand, suspensions containing higher amounts of NSP in MetA resin exhibited more than one plasmon absorption band. Fig. 3(a)–(c) show the UV–vis spectra of suspensions containing 300 ppm NSP prepared at different temperatures. Initially, only one band, centred at 440 nm, was present. The development of this band showed a marked red shift, indicative of an increase in the

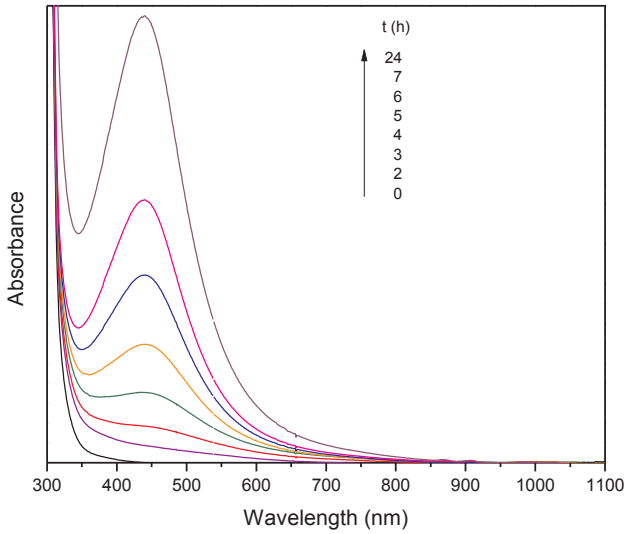

Fig. 2. UV–vis absorption spectra of a suspension containing 150 ppm NSP in MetA at different reaction times. A solution of $AgNO_3$ in ACN was added to MetA and the formation of NSP was carried out at room temperature.

average NSP size. As the reaction proceeded, a shoulder was clearly observed after 8 h reaction at room temperature (Fig. 3a). After 10 h reaction the suspension exhibited a broad absorption band in the range 360–1100 nm and the colour of the colloids changed from pale yellow to dark green. The dark colour suggests that the fine NSP initially formed gradually agglomerate into certain stable size distribution (Henglein and Giersig, 1999). As will be discussed later, the photothermal effect is enhanced when the plasmonic band of the NSP matches the solar emission spectrum. Thus, it is important to prepare nanostructures that exhibit a wide absorption range. The effect of reaction temperature on the formation of NSP in suspensions containing 300 ppm NSP is illustrated in Fig. 3(b) and (c). UV–vis spectra taken at

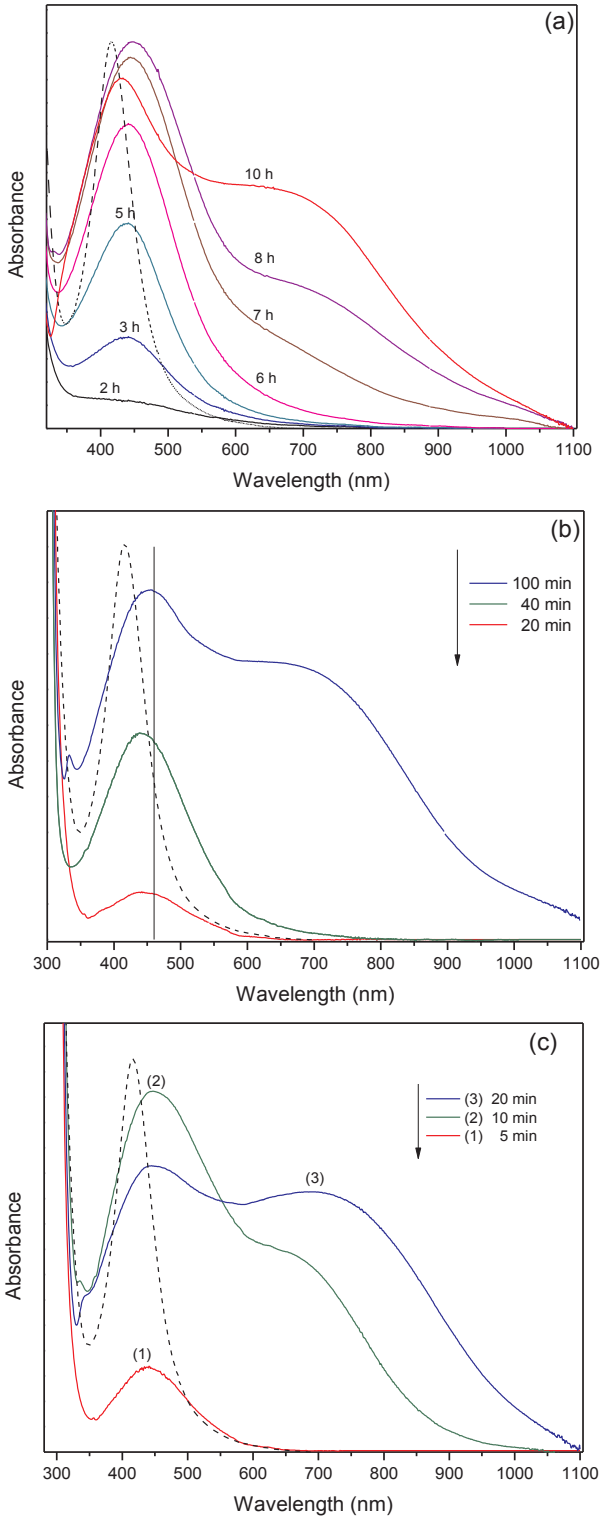

Fig. 3. UV–vis absorption spectra of a suspension containing 300 ppm NSP in MetA at different reaction times (solid lines). Solutions of $AgNO_3$ in ACN were added to MetA and the formation of NSP was carried out at (a) room temperature (21 ± 1 °C), (b) 40 °C, and (c) 60 °C. The dashed line is the UV–vis spectrum of a suspension containing 300 ppm spherical NSP prepared in MetB as described in Asmussen and Vallo (2015).

regular intervals show that a fast process took place initially since an absorption band appeared at ~420 nm within a few minutes after mixing the reagents. Once the reduction of silver ions is completed, the high temperature promotes a faster particle aggregation, which is reflected by the red shift of the band and a new shoulder arising from the plasmon resonance of the aggregates. Dark green silver suspensions with a broad absorption band were obtained after about 90 and 20 min at 40 and 60 °C respectively. As stated by Miés theory spherical NNP exhibit a single plasmon absorption band whereas anisotropic NNP exhibit multiple plasmonic bands (Quinten, 2011). The three peaks at 335, 440, and 700 nm in Fig. 3(b) and (c) are associated to the presence of triangular nanoparticles (Shinde et al., 2013; Jin et al., 2001). The band centred at ~440 nm results from combined effect from the absorption of small spherical NSP and the out-of-plane polarization of truncated triangular NSP. The band centred at ~700 nm arises from the interaction of truncated triangular NSP with light (Si et al., 2011). This band is relatively broad due to combination of NNP pairs with variable degrees of overlap. Results presented in Fig. 3(a)–(c) show that suspensions containing 300 ppm NSP, synthesized with ACN, display an absorption band that covers both the visible and near-IR regions. This feature enables them to interact with photons over a wide spectral range for and efficient harvesting of solar energy.

Suspensions prepared with 1000 and 2000 ppm NSP were dark red and yielded a single peak in the UV–vis spectra (not shown here) similar to those in Fig. 2. Results reported by previous researchers show that the morphology of NSP strongly depends on the reaction conditions such as the concentration of silver precursor and reducing agent, temperature, as well as the presence of surfactant agents which interact selectively with different crystallographic planes of silver. Yu and Yam (2005) found that at fixed concentration of $AgNO_3$ an increase in the concentration of (n-hexadecyl trimethylammonium bromide) surfactant resulted in a shape evolution of NSP from spheres to cubes and spheres again. Dong et al. (2010) shown that the formation of the silver triangular plates was dependent on the proportion of reducing agent sodium borohydride used in the synthesis. At low concentration of sodium borohydride spherical and rodlike silver NSP were obtained. At medium concentration of sodium borohydride the product was triangular plates. At high concentration of sodium borohydride spherical nanoparticles were obtained. Xiong et al. (2006) demonstrated that the growth of silver nanoplates requires the existence of stacking defects, and the formation of nanoplates is possible only if the reduction process is slow. Under a reduction process slow enough, nucleation and growth occur under kinetic control and, consequently, are produced. Conversely, nanoplates are not formed if the reduction process is fast. In this study; suspensions of NSP were prepared by mixing 1 g of a 3 wt% solution of $AgNO_3$ in ACN with the appropriate amount of MetA (Table 1). As the amount of NSP is increased the proportion of the MetA and the related amount of reducing agent (BHT) decrease (Table 1), which contributes to a decrease in the reduction rate. On the other hand, as the amount of NSP increases the mobility of the reacting medium also increases because of the higher proportion of the low-viscosity ACN monomer (Table 1). The net effect of an increased mobility of the reacting medium is an increase in the reduction rate. Consequently, under these experimental conditions the minimum reduction rate is expected to occur at an intermediate content of NSP. The formation of spherical particles at 150, 1000 and 2000 ppm NSP and triangular plates at 300 ppm NSP is attributed to different reduction rates among the systems, in agreement with Xiong et al. (2006).

The formation of spherical NSP in the MetB monomer has been reported previously (Asmussen and Vallo, 2015). Nanocomposites containing 300 ppm spherical NSP in MetB, prepared as reported previously, were used in this study for comparative purposes (See UV–vis spectra in Fig. 3).

3.2. TEM microscopy

Representative TEM micrographs of methacrylate resins containing 300 ppm NSP are shown in Fig. 4(a)–(e). Panoramic views shown in Fig. 4(a) and (b) reveal that partly agglomerated NSP with varying morphology and very broad size distribution are formed. As described

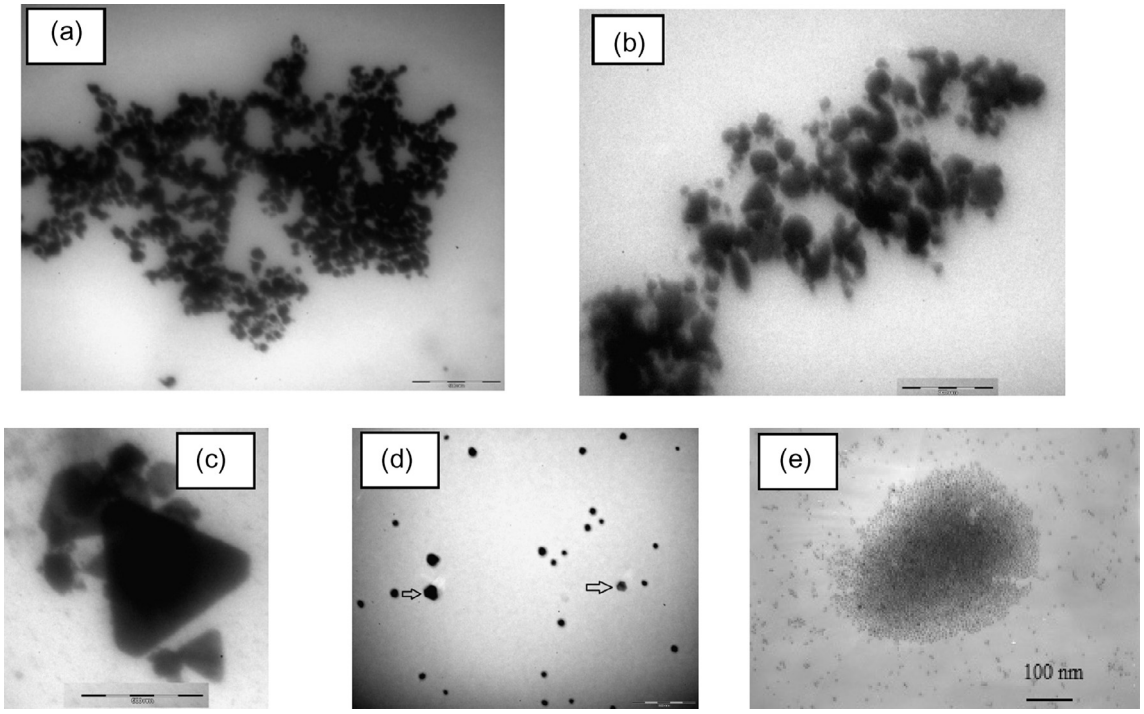

Fig. 4. TEM images of suspensions containing 300 ppm NSP in the presence of ACN. (a)-(b) are panoramic views of the NSP. At higher magnification the presence of triangles (c) and truncated triangular NSP (d) is more clearly seen. Image (e) is a suspension of 300 ppm spherical NSP prepared in MetB as described in Asmussen and Vallo (2015).

in the experimental section, the NSP were deposited on a carbon-coated TEM grid by casting on it a drop of the solution of methacrylate resin/ethanol and allowing the evaporation of ethanol. It is probable that these self-assembled structures were not generated in solution but formed on the grid during the ethanol evaporation which causes some of the NNP to aggregate. In agreement with UV–vis spectra in Fig. 3, TEM images revealed the presence of triangular and truncated triangular NSP. Fig. 4(c) and (d) are selected pictures showing clearly these morphologies.

3.3. Polymerization of the suspension of NSP

Nanocomposites were prepared by polymerization of resins having the composition shown in Table 1. Suspensions of NSP prepared as described previously were activated with 1 wt% BPO and polymerized in an oven at 80 °C. Fig. 5 illustrates the conversion of methacrylate groups monitored by NIR for different sample thickness. It is seen that the polymerization proceeds very rapidly after the inhibitors are consumed. For the 0.5 and 1 mm thick samples, the conversion achieved was lower than that in the 2 mm thick sample. This effect is attributed to a higher temperature rise in the thickest sample due to the exothermic polymerization reaction (Vallo, 2002). UV–vis spectra taken after polymerization were identical to those of the initial suspensions, indicating that the morphology of the suspensions was not affected by the polymerization of the resin. Fig. 6 shows pictures of polymerized nanocomposites containing different amounts of NSP.

3.4. Photothermal conversion studies

Studies concerning the photothermal conversion during irradiation of suspensions of noble metal NNP have been commonly carried out by the continuous monitoring of temperature increase (Richardson et al., 2009; Cole et al., 2009; Chen et al., 2010). The local temperature evolution arising from laser irradiation of suspensions of gold NNP in water has been accurately measured by placing a thermocouple in the suspensions (Richardson et al., 2009; Cole et al., 2009; Chen et al., 2010). In this study, the photothermal conversion of nanocomposites containing NSP was examined by monitoring the temperature evolution in 2-mm thick plates during irradiation with different light sources. We first studied the photothermal conversion of nanocomposites under irradiation with narrow band LEDs. The temperature rise in nanocomposites during irradiation with violet, blue, green and red LEDs are presented in Fig. 7(a)–(d) respectively. It is seen that all traces exhibited a similar trend. The temperature experienced a rapid rise and then reached a plateau after about 20 min. For a given nanocomposite, the maximum temperature reached during irradiation increased when the wavelength of the LED source decreased. A maximum temperature increase of 24 °C occurred in the sample containing 300 ppm NSP,

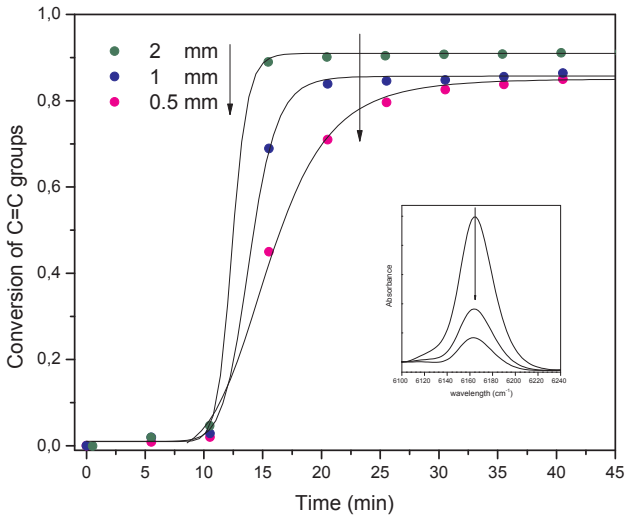

Fig. 5. Extent of reaction reached in suspensions containing 300 ppm NSP activated with BPO. The polymerization was carried out at 80 °C. The specimens were 10-mm diameter. Typical decrease of NIR bands of the methacrylate groups are also shown.

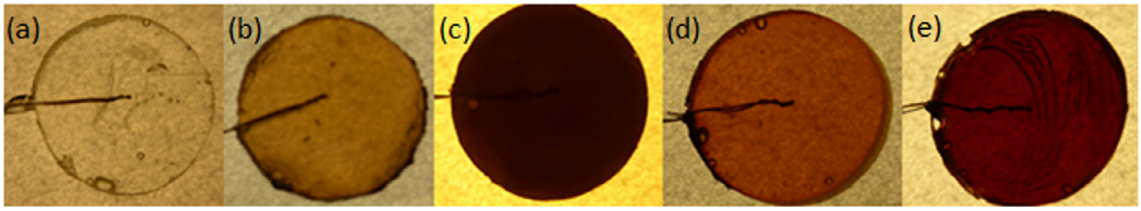

Fig. 6. Pictures showing polymerized samples of MetA resin (a), nanocomposites prepared with 150 ppm NSP in ACN (b), 300 ppm NSP in ACN (c) 300 ppm NSP in ethanol as described in Asmussen and Vallo (2015) (d) and 1000 ppm NSP in ACN (e).

synthesized with ACN, irradiated with the violet LED (410 nm). In addition, the difference in temperature rise among samples irradiated with the same LED was markedly affected by the LED wavelength. The highest and lowest values of temperature reached in samples irradiated with the 410 nm LED were 47 and 40 °C while less significant differences were observed in the values of temperature reached under irradiation at 630 nm. The highest temperature is reached when the overlap between the plasmonic band of the NNP and the spectral distribution of the light source is optimized. Conversely, when the absorption band is shifted away from the wavelength range of the LED, the light absorption becomes smaller, leading to the reduction in the final temperature.

Figs. 8 and 9 show the spectral distribution of the white LED and the temperature evolution during irradiation of the nanocomposites with white light respectively. This LED was used in the experiments because it displays a spectral distribution that, at this stage of our research, enables us to reach definite conclusions about the suitability of the synthesized nanocomposites as absorber materials for solar energy collectors. If we consider that the starting temperature was 23 °C, a remarkable net temperature increase of 92 °C was obtained in the composite containing 300 ppm NSP synthesized with ACN. The values of temperature reached in different nanocomposites are explained in terms of the content of NNP and the combined effect of size, morphology and aggregation of the NNP, which affect the efficiency of the photothermal conversion of electromagnetic energy into heat. Measurements performed in nanocomposites derived from NSP-MetB enabled us to compare the effect of the morphology of the NNP on the photothermal conversion efficiency.

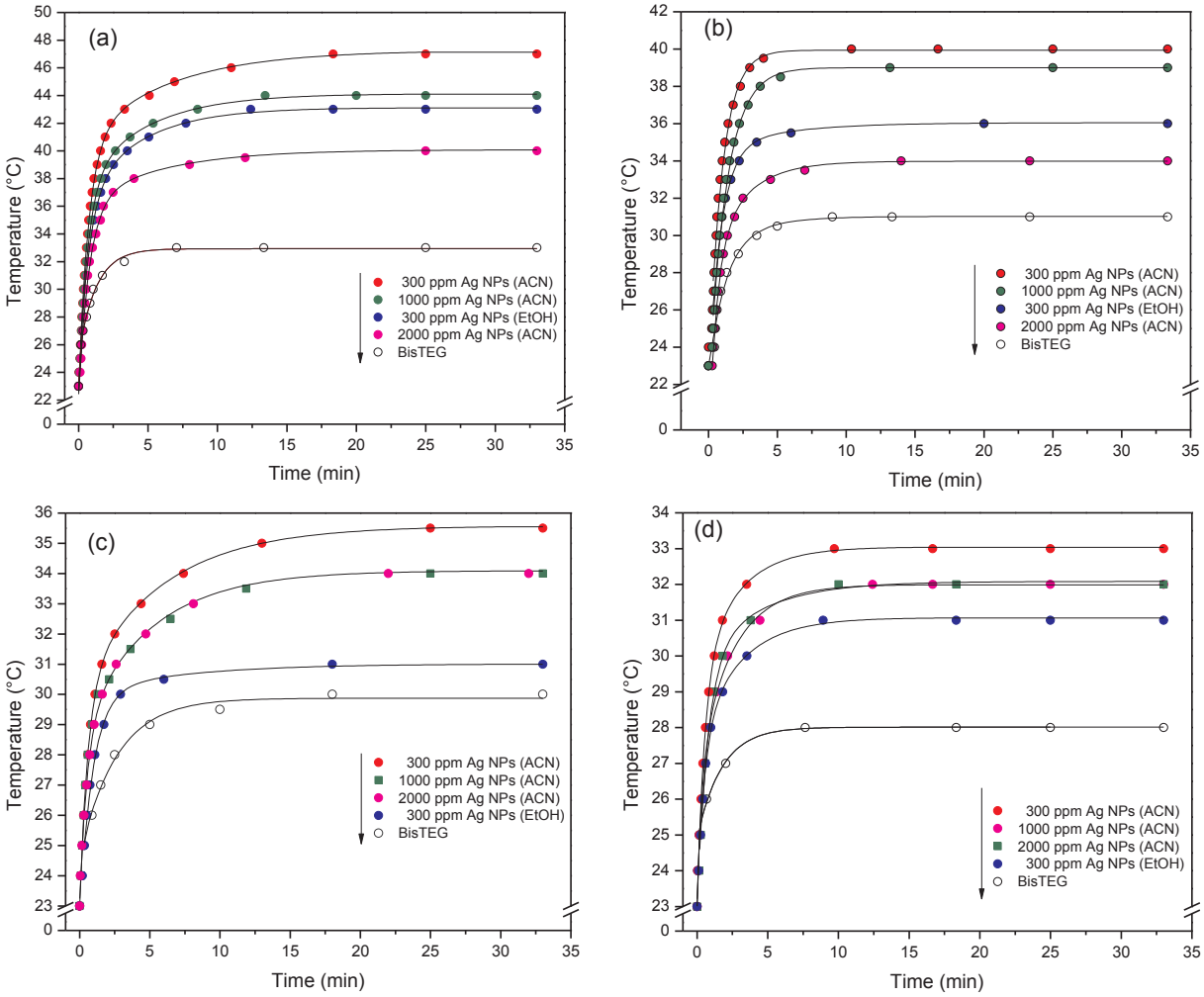

Fig. 7. Temperature progress during irradiation of nanocomposite specimens containing different amounts of NSP. The wavelength of the LEDs was (a) 410 nm, (b) 465 nm, (c) 520 nm and (d) 630 nm. The power of the LEDs was 50 mW. The specimens were 10 mm diameter and 2 mm thick. Specimens were 2 mm thick and 10 mm diameter.

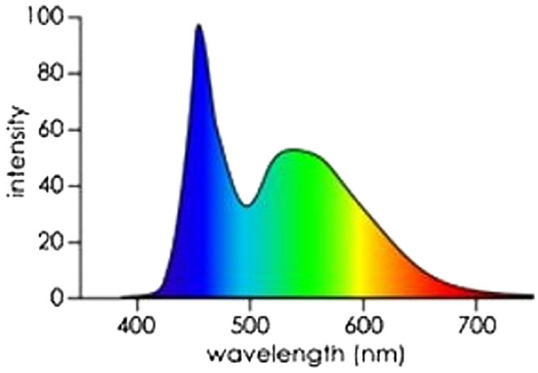

Fig. 8. Spectral power distribution of the white LED.

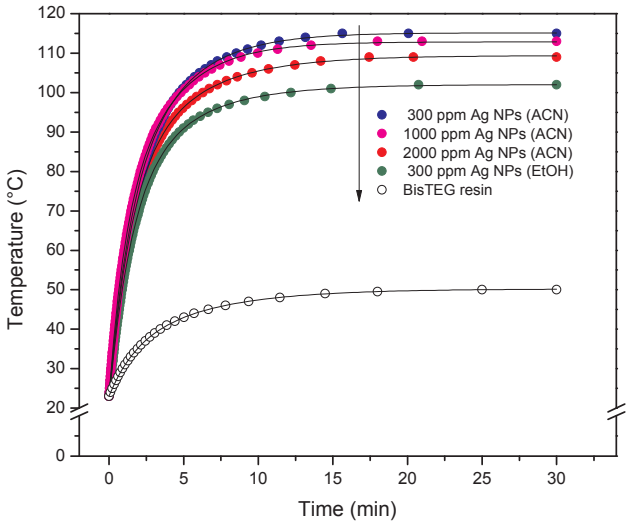

Fig. 9. Temperature progress during irradiation of nanocomposites. The power of the LEDs was 7 W. The specimens were 2 mm thick and 20 mm diameter (see Fig. 6).

When a noble metal nanoparticle is irradiated, part of the incident light is scattered, while the other part gets absorbed and finally dissipated into heat. The balance between absorption and scattering depends on the size and shape of the nanoparticle. The effect of particle morphology on local heating under laser irradiation has been reported in previous research (Baffou et al., 2009; Mackey et al., 2014). Baffou et al. investigated the heating efficiency of NNP (spheres and nanorods) and planar nanostructures (circular plates and triangles) immersed in aqueous medium (Baffou et al., 2009). Theoretical calculations showed that the heat generation by gold NNP irradiated at its localized surface plasmon resonance arises mainly from the surface of the particles facing the radiation. Interestingly, the major part of spherical nanoparticle is buried; therefore, it does not contribute to heating. Conversely, for elongated nanorods having identical volume than a sphere this shielding effect is less marked and almost the entire volume of the nanoparticle contributes to the heating process. This explains the higher temperature reached in suspensions of nanorods compared with that reached in suspensions of nanospheres. Moreover, as a result of a reduced shielding effect the heating power of planar NNP (circular disks and triangles) was markedly greater than that of spheres and nanorods. In addition, Mackey et al. (2014) reported that the amount of heat generated by gold NNP upon laser irradiation is also governed by the distance at which the electric field extends away from the nanoparticle surface. The authors also found that the presence of nanoparticle aggregates contributes to increase the heating of the medium. In agreement with results reported by the aforementioned studies, the higher temperature reached in nanocomposites containing 300 ppm NSP synthesized in ACN is attributed to the presence of planar nanostructures. On the other hand, in nanocomposites containing spherical particles the major part of the nanoparticle surfaces is not exposed to light and, therefore, they do not participate in the photothermal conversion process. The lower values of temperature reached in nanocomposites containing 1000 and 2000 ppm NSP is attributed to both a spherical morphology and a light screening effect (Asmussen and Vallo, 2015). The scattering and absorption of light by the NSP produce a marked attenuation of the light intensity which results in a decreased heating of the NSP.

Results obtained in this study, demonstrate that the maximum temperature rise under light irradiation occurs in nanocomposites containing 300 ppm NSP, prepared in MetA resin and using a small amount of ACN monomer to dissolve silver nitrate. These experimental conditions result in a particular morphology of the NSP that optimizes the absorption of electromagnetic energy and its conversion into heat. The absorber material can be fabricated by the technique of resin casting, in which the liquid suspension of NSP containing benzoyl peroxide is poured into a mould of desired shape and a solid piece is obtained after 20–30 min polymerization at 80 °C followed by a post-curing treatment at 120 °C for 20 min. Alternatively, the resin can be used as coating for a given substrate and polymerized as described above or photocured in the presence of adequate photoinitiators (Asmussen and Vallo, 2015).

4. Conclusion

MetA methacrylate resin containing NSP can be easily prepared by dissolving silver nitrate with acrylonitrile monomer.

The synthesis conditions were adjusted in order to broaden the plasmon absorption band of the resultant nanoparticles. Suspensions containing 300 ppm NSP exhibited wide absorption spectra (360–1100 nm) nm with three peaks at 335, 440, and 700 associated to the presence of triangular NSP.

The temperature reached during irradiation of nanocomposites showing a broad absorption band was 115 °C while that of the nanocomposites exhibiting a single peak was 102 °C.

The suspensions of NSP can be shaped by various routes of processing of polymers.

Nanocomposites derived from MetA-NSP are attractive absorber materials for solar thermal collectors.

Acknowledgements

This work was financially supported by the National Scientific and Technical Research Council (CONICET) (PUE Project 22920160100073CO and PIP Project 20150100594).

References

Aberasturi, D.J., Serrano-Montes, A.B., Liz-Marzán, L.M., 2015. Modern applications of plasmonic nanoparticles: from energy to health. Adv. Opt. Mater. 3, 602–617.
Asmussen, S.V., Vallo, C.I., 2015. Synthesis of silver nanoparticles in surfactant-free light-cured methacrylate resins. Coll. Surf. A: Physicochem. Eng. Aspects 466, 115–124.
Baffou, G., Quidant, R., 2013. Thermo-plasmonics: using metallic nanostructures as nano-sources of heat. Laser Photon. Rev. 7, 171–187.
Baffou, G., Quidant, R., Girard, C., 2009. Heat generation in plasmonic nanostructures: influence of morphology. Appl. Phys. Lett. 94, 153109.
Barrera, E., González, F., Velásquez, C., Ojeda, M.L., Sánchez, M., Rentería-Tapia, V., 2018. Broadband solar absorption enhancement in a silver-epoxy nanocomposite for use as selective coating. Plasmonics 1–11.
Beikircher, T., Möckl, M., Osgyan, P., Streib, G., 2015. Advanced solar flat plate collectors with full area absorber, front side film and rear side vacuum superinsulation. Sol. Energy Mater. Sol. Cells 141, 398–406.
Chen, H., Shao, L., Ming, T., Sun, Z., Zhao, C., Yang, B., Wang, J., 2010. Understanding the photothermal conversion efficiency of gold nanocrystals. Small 20, 2272–2280.
Cole, J.R., Mirin, N.A., Knight, M.W., Goodrich, G.P., Halas, N.J., 2009. Photothermal efficiencies of nanoshells and nanorods for clinical therapeutic applications. J. Phys. Chem. C 113, 12090–12094.

Dong, X., Ji, X., Jing, J., Li, M., Li, J., Yang, W., 2010. Synthesis of triangular silver nanoprisms by stepwise reduction of sodium borohydride and trisodium citrate. J. Phys. Chem. C 114, 2070–2074.
Fan, D., Li, Q., Chen, W., Zeng, J., 2017. Graphene nanofluids containing core-shell nanoparticles with plasmon resonance effect enhanced solar energy absorption. Sol. Energy 158, 1–8.
Granqvist, C.G., Niklasson, G.A., 2018. Solar energy materials for thermal applications: a primer. Sol. Energy Mater. Sol. Cells 180, 213–226.
Henglein, A., Giersig, M., 1999. Formation of colloidal silver nanoparticles: capping action of citrate. J. Phys. Chem. B 103, 9533–9539.
Holm, V.R.A., Greve, M.M., Holst, B., 2017. A theoretical investigation of the optical properties of metal nanoparticles in water for photo thermal conversion enhancement. Energy Convers. Manage. 149, 536–542.
Hong, S.U., Jin, J.H., Won, J., Kang, Y.S., 2000. Polymer-salt complexes containing silver ions and their application to facilitated olefin transport membranes. Adv. Mater. 12, 968–971.
Jeon, J., Park, S., Lee, B.J., 2016. Analysis on the performance of a flat-plate volumetric solar collector using blended plasmonic nanofluid. Sol. Energy 132, 247–256.
Jin, R., Cao, Y.W., Mirkin, C.A., Kelly, K.L., Schatz, G.C., Zheng, J.G., 2001. Photo induced conversion of silver nanospheres to nanoprisms. Science 294, 1901–1903.
Khan, M.M.A., Ibrahim, N.I., Mahbubul, I.M., Ali, H., Saidur, M.R., Al-Sulaiman, F.A., 2018. Evaluation of solar collector designs with integrated latent heat thermal energy storage: a review. Sol. Energy 166, 334–350.
Klein, A., Oreski, G., Resch-Fauster, K., 2017. Applicability of technical biopolymers as absorber materials in solar thermal collectors. Sol. Energy 153, 276–288.
Mackey, M.A., Ali, M.R.K., Austin, L.A., Near, R.D., El-Sayed, M.A., 2014. The most effective gold nanorod size for plasmonic photothermal therapy: theory and in vitro experiments. J. Phys. Chem. B 118, 1319–1326.
Mason, J.J., 1983. Selective absorbing surfaces in practice. Surf. Technol. 20, 339–356.
Mishra, Y.K., Mohapatra, S., Chakravadhanula, V.S.K., Lalla, N.P., Zaporojtchenko, V., Avasthi, D.K., Faupel, F., 2010. Synthesis and characterization of Ag-polymer nanocomposites. J. Nanosci. Nanotechnol. 10, 2833–2837.
O'Hegarty, R., Kinnane, O., McCormack, S.J., 2016. Review and analysis of solar thermal facades. Sol. Energy 135, 408–422.
Qin, C., Kang, K., Lee, I., Lee, B.J., 2017. Optimization of a direct absorption solar collector with blended plasmonic nanofluids. Sol. Energy 150, 512–520.
Quinten, M., 2011. Optical Properties of Nanoparticle Systems Mie and Beyond. Wiley-VCH, Germany.
Richardson, H.H., Carlson, M.T., Tandler, P.J., Hernandez, P., Govorov, A.O., 2009. Experimental and theoretical studies of light-to-heat conversion and collective heating effects in metal nanoparticle solutions. Nano Lett. 9, 1139–1146.
Sarsam, W.S., Kazi, S.N., Badarudin, A., 2015. A review of studies on using nanofluids in flat-plate solar collectors. Sol. Energy 122, 1245–1265.
Shang, M., Zhang, S., Li, N., Gu, X., Li, L., Wang, Z., 2017. Di-functional nanocomposite films for efficient conversion and storage of solar energy. Sol. Energy Mater. Sol. Cells 164, 188–192.
Sharaf, O.Z., Kyritsis, D.C., Al-Khateeb, A.N., Abu-Nada, E., 2018. Effect of bottom surface optical boundary conditions on nanofluid-based DASC: parametric study and optimization. Sol. Energy 164, 210–223.
Shinde, V.V., Jadhav, P.R., Kim, J.H., Patil, P.S., 2013. One-step synthesis and characterization of anisotropic silver nanoparticles: application for enhanced antibacterial activity of natural fabric. J. Mater. Sci. 48, 8393–8401.
Si, G., Shi, W., Li, K., Ma, Z., 2011. Synthesis of PSS-capped triangular silver nanoplates with tunable SPR. Colloids Surf. A 380, 257–260.
Thirugnanasambandam, M., Iniyan, S., Goic, R., 2010. A review of solar thermal technologies. Renew. Sustain. Energy Rev. 14, 312–322.
Tian, Y., Zhao, C.Y., 2013. A review of solar collectors and thermal energy storage in solar thermal applications. Appl. Energy 104, 538–553.
Vallo, C.I., 2002. Theoretical prediction and experimental determination of the effect of mold characteristics on temperature and monomer conversion fraction profiles during polymerization of a PMMA-based bone cement. J. Biomed. Mater. Res. B 63, 627–642.
Wang, X., He, Y., Liu, X., Shi, L., Zhu, J., 2017a. Investigation of photothermal heating enabled by plasmonic nanofluids for direct solar steam generation. Sol. Energy 157, 35–46.
Wang, X., He, Y., Liu, X., Cheng, G., Zhu, J., 2017b. Solar steam generation through bio-inspired interface heating of broadband-absorbing plasmonic membranes. Appl. Energy 195, 414–425.
Xiong, Y., Washio, I., Chen, J., Cai, H., Li, Z.-Y., Xia, Y., 2006. Poly(vinyl pyrrolidone): a dual functional reductant and stabilizer for the facile synthesis of noble metal nanoplates in aqueous solutions. Langmuir 22, 8563–8570.
Yu, X., Xuan, Y., 2018. Investigation on thermo-optical properties of CuO/Ag plasmonic nanofluids. Sol. Energy 160, 200–207.
Yu, D., Yam, V.W.-W., 2005. Hydrothermal-induced assembly of colloidal silver spheres into various nanoparticles on the basis of HTAB-modified silver mirror reaction. J. Phys. Chem. B 109, 5497–5503.
Zhang, Z., Han, M., 2003. One-step preparation of size-selected and well-dispersed silver nanocrystals in polyacrylonitrile by simultaneous reduction and polymerization. J. Mater. Chem. 13, 641–643.